Temporal Evolution of Wavelength and Orientation of Atmospheric Canopy Waves

Alejandro Espinoza-Ruiz[1], Julia E. Colombini[1], Emily K. Everton[1], Pierre Dérian[2], and Shane D. Mayor[1]

[1] California State University Chico, Chico CA 95929, USA, sdmayor@csuchico.edu
[2] Independent Researcher, Nantes, France, pierre.derian@gmail.com

Abstract. We describe an algorithm that can be applied to horizontally scanning atmospheric aerosol lidar data to determine canopy wave orientation and wavelength objectively. We applied it to over 1500 images of canopy waves from 53 episodes collected during the Canopy Horizontal Array Turbulence Study (CHATS). By doing so, we created time-series of wavelength and orientation. Results from episode 25 from April 30, 2007, are presented.

Keywords: boundary layer processes · image processing · canopy waves · gravity waves · stable boundary layers · elastic backscatter aerosol lidars

1 Introduction

Canopy waves are small-scale vertical oscillations of the stable atmospheric boundary layer that occur near the top of forest canopies due to the drag of the trees. An inflection point in the mean wind speed profile results in Kelvin-Helmholtz instability that excites the waves. If the waves increase in amplitude over time, they may break and generate turbulence that is an efficient transporter of heat, trace gases, and momentum. We are studying the temporal evolution of atmospheric canopy waves using scanning lidar data in an effort to better understand the factors that control formation and dissipation or transition to turbulence.

We applied an algorithm (created by P. Dérian) to horizontally scanning aerosol lidar images to objectively determine the wavelength and orientation of the wave crests. We applied it to scans from the Raman-shifted Eye-safe Aerosol Lidar (REAL) [1] from the Canopy Horizontal Array Turbulence Study (CHATS) [2]. The data set includes 53 episodes of canopy waves distributed over a three-month period [3]. Episodes ranged from a few minutes in duration to more than an hour in some cases. Therefore, the number of scans (or frames) in an episode ranged from 7 to 148. The algorithm determines a single salient wavelength and orientation angle of the waves from a square subset of pixels that is typically hundreds of meters wide in each dimension.

Mifsud et al. [4] demonstrated that the objectively determined wavelengths and orientations were very close to subjectively determined values. In that work, only one frame per episode was examined. We applied the algorithm to all frames of all episodes to determine the temporal evolution of wavelength and orientation. By applying the algorithm to all frames in an episode we can efficiently monitor the wave characteristics over time. Unfortunately, due to the large amount of natural variability from case to case, we have yet to find a good way to display and summarize the time-series results of all 53 episodes. Therefore, in this paper we show just one of the 53 episodes.

Wavelength is the distance from one wave crest to the next. The orientation is the angle between the axis of the wave crests and north. For example, wave crests running from west to east have a 90° orientation. Wave crests running from the NW to the SE have a 135° orientation. In general, the orientation of the waves is perpendicular to the wind direction. In other words, the wave crests are *wind perpendicular* bands (in contrast to *wind parallel* features such as plumes).

2 Algorithm

The algorithm computes an autocorrelation function (ACF) for a rectangular subset of pixels in a horizontal lidar scan. The subset of pixels is called a region of interest (ROI)(Fig. 1, left) that must be manually set to avoid areas with hard target returns and non-wave aerosol features such as dust plumes. The ACF (Fig. 1, right) reveals smooth bands of positive correlation that are spaced at intervals of wavelength and oriented the same as the waves. To extract a single orientation and wavelength from the ACF, the pixels are averaged in narrow angular sectors (Fig. 2, left) and concentric rings (Fig. 3, left), respectively. These averages, as functions of angle and radius, contain local maxima that correspond to the orientation and wavelength (Fig. 2, right and Fig. 3, right). We apply this algorithm to each lidar scan in an episode to construct the time series of wavelength and orientation.

3 Results

We chose to show episode 25 (30 April 2007) because the wavelength changes significantly and steadily starting at 30 m and increasing to over 80 m in 11 minutes. (Note: the range of wavelengths over all 53 episodes ranges from about 30 m to 100 m.) After 12:47, the objectively determined wavelengths becomes erratic as the episode ends and the flow begins to reverse. In the beginning of this episode the wind was from the SW. The erratic excursions in wavelength after 12:47 are not likely to be wavelengths as the waves are loosing coherence during that time. Fig. 4 shows a subset of 4 of the 31 frames centered on the instrumented 30-m tower.

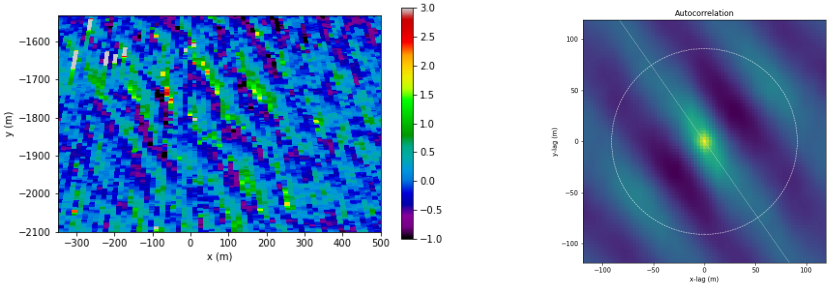

Fig. 1: Left panel: a subset of pixels from a full lidar scan featuring the canopy waves of interest. Right panel: The 2D autocorrelation function of the image in the left panel.

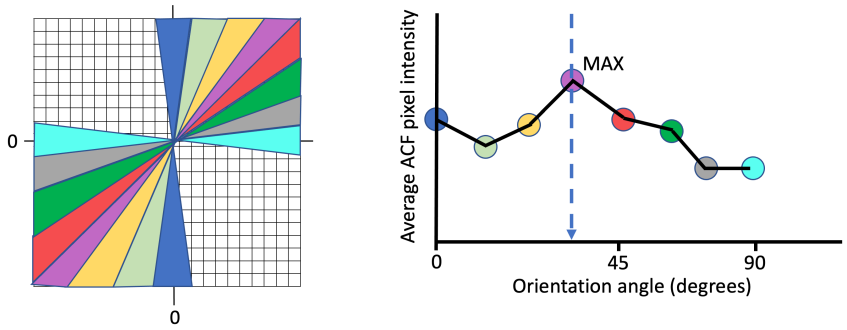

Fig. 2: Left panel: ACF pixels are averaged in narrow angular sectors to find the wave orientation. Right panel: The average of the sectors as a function of angle.

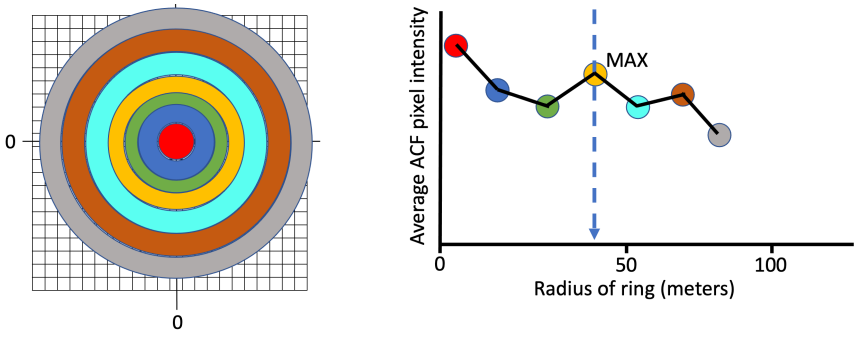

Fig. 3: Left panel: ACF pixels are averaged in circular rings to find the wavelength. Right panel: The average of the pixels in the rings as a function of radius.

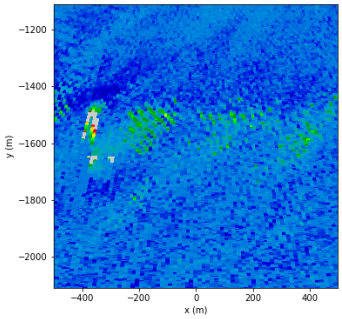

(a) Time: 12:36:26 UTC

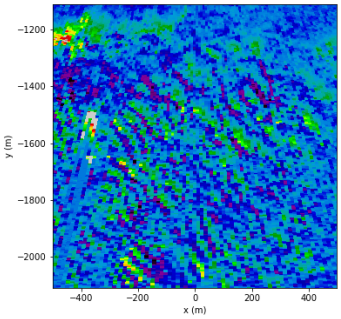

(b) Time: 12:41:59 UTC

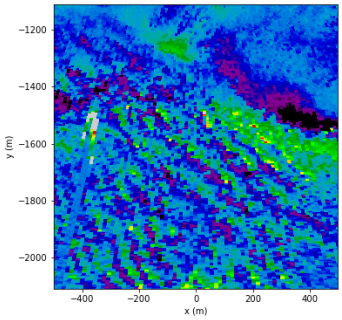

(c) Time: 12:48:33 UTC

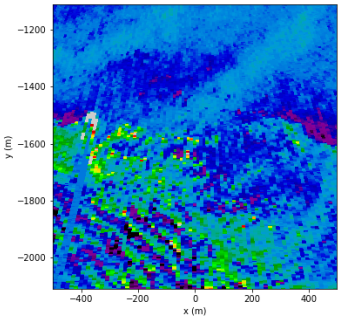

(d) Time: 12:51:34 UTC

Fig. 4: A subset of 4 of 31 lidar images of the canopy waves in episode 25. Each area is 1 km × 1 km and centered on the location of the CHATS 30-m vertical tower. The green colors represent higher aerosol backscatter intensity. The lidar data have been high-pass median filtered in their native polar coordinate system.

The first frame (12:36:26) reveals very fine-scale waves limited to a relatively small area. The second frame (12:41:59) shows that the waves have grown dramatically in terms of area extent and wavelength. The third frame (12:48:33) shows a band of aerosol advecting in from the NE which is associated with the end of the episode. The fourth frame (12:51:34) shows that the aerosol band has moved across the center of the images where the tower is located.

The algorithm successfully captures the increase in wavelength during this episode (see top panel in Fig. 5). The wave orientations (see bottom panel in Fig. 5) are fairly consistent (about 145°) over the first 10 minutes with the exception of one data point at 12:38. The orientations near the end of the episode change. We cannot detect rotation of the wave crests during the end of the episode, so the last 10 data points may not be meaningful. (Note, 90° at the last data point would be east-west orientation.)

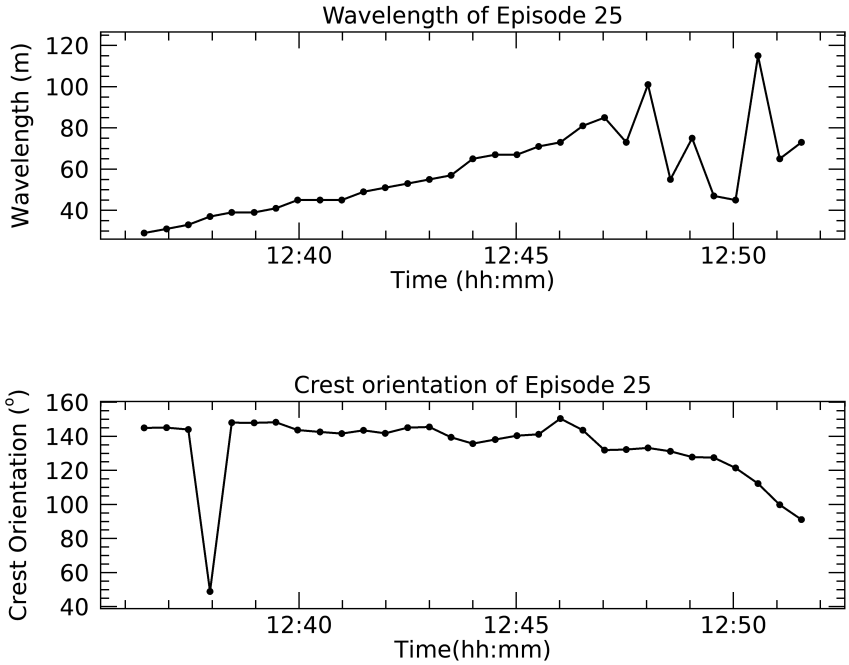

Fig. 5: Time series of wavelength (top) and orientation (bottom) for episode 25.

4 Conclusions

Scanning aerosol lidar data can reveal important quantitative information on microscale wave structure and evolution. However, algorithms are necessary to extract that quantitative information. Here, we applied a new algorithm to extract wavelength and orientation from image sequences in order to produce time-series.

We have learned that it is important to restrict the region of interest to avoid hard-target and non-wave aerosol features. The algorithm will only provide reliable results when a single wave train is in the ROI. We have occasionally observed two wave trains with different wavelengths and orientations present simultaneously. In these cases, the algorithm can only lock onto one or the other, and it may hop back and forth erratically.

In the future, we plan to explore whether any consistent trends exist and whether the wavelength and orientation can be linked to other variables such as wind velocity and static stability as measured by in situ sensors on the tower. We also plan to objectively delineate the individual wave crests and their phase propagation velocity. Doing so will allow us to track all wave crests in an image and explore the temporal and spatial evolution of the waves in unprecedented detail.

Acknowledgements This material is based upon work supported by the National Science Foundation under Grant AGS 2054969. The first three coauthors are undergraduates majoring in environmental sciences at California State University Chico.

References

1. Mayor, S. D., S. M. Spuler, B. M. Morley, E. Loew: Polarization lidar at 1.54-microns and observations of plumes from aerosol generators. Opt. Eng., **46**, 096201 (2007).
2. Patton, E. G. et al.: The Canopy Horizontal Array Turbulence Study (CHATS), Bull. Amer. Meteorol. Soc. **92**, 593–611 (2011).
3. Mayor, S. D.: Observations of microscale internal gravity waves in very stable atmospheric boundary layers over an orchard canopy. Agric. For. Meteorol. 244-245, 136–150 (2017).
4. Mifsud, K. E., M. Iqbal, P. Dérian, S. D. Mayor: Objective determination of wavelength and orientation of atmospheric canopy waves. In: Fall meeting of the American Geophysical Union, 16 December, New Orleans, LA. Poster presentation A45C-1867 (2021).